SUPPLEMENTAL METHODS

Neural Signal Processing and Decoding: Neural signals recorded at 30 kHz on each of 192 channels were band-pass filtered (250-3000 Hz), common average referenced, and down-sampled to 15 kHz in real time. To perform the common average reference, we selected the 60 channels on each array that had the lowest signal power (variance) and averaged them together to yield an array-specific common average reference, which was then subtracted from each channel. At every 20 millisecond time step, 192 threshold crossing rates and 192 high frequency power values were computed using the past 20 ms of data for each channel and concatenated into a 384 × 1 feature vector. Threshold crossing rates were defined as the number of times that the voltage time series on a given channel crossed a channel-specific threshold from above (-4.5 × RMS), divided by the width of the time window (which could be less than 20 ms for FES blocks due to stimulus artifact "blanking"). High frequency power was defined as the average power during that window on a band-pass filtered channel. For FES blocks, to ensure that a stimulation artifact did not affect our features, we "blanked" the channels by ignoring all data for a 15 ms window during which stimulation occurred. This resulted in one or two shorter time windows every 80 ms (with the minimum window length being 5 ms).

At each time step, we mapped the neural features to a "control" vector with the equation $u_t=Df_t$, where f_t is a 384 × 1 neural feature vector, D is an M x 384 decoding matrix, and u_t is a M × 1 decoded control vector, with M denoting the number of decoded dimensions (for single-joint movements, M is 1; for 2 and 3-joint movements, M is 2 and 3, respectively). To calibrate the decoding matrix using attempted movement and/or closed-loop virtual reality blocks, we made the assumption that neural features were linearly tuned to a joint angle error vector of unit magnitude: $c_t=(g_t-p_t)/||g_t-p_t||$, where g_t is a vector of the target joint angles and p_t is a vector of the virtual arm's current joint angles. To ensure that each joint was weighted equally, joint angles were first normalized by dividing by the range of angles spanned by the targets.

To calibrate the optimal linear estimator, we first found the top 120 features that were most highly correlated with c_t (measured by Pearson's *r*). We then assumed that the reduced neural feature vector f_t linearly encodes c_t:

$$f_t = Ec_t + \varepsilon_t,$$

where f_t is the 120 x 1 reduced neural feature vector that has been z-scored to have zero mean, E is a 120 x M encoding matrix containing preferred directions, c_t is the M x 1 joint error vector (called the decoder calibration signal in Supplementary Figure 2), and ε_t is an 120 x 1 noise vector (where $\varepsilon_t \sim N(0, \Sigma)$). We used least squares regression to estimate E and Σ using all 20 ms samples that occurred between 0.3 to 1.5 seconds after the start of each trial. We then computed the optimal linear estimator using the equation $D = (E^T\Sigma^{-1}E)^{-1}E^T\Sigma^{-1}$ (this procedure has been called "full OLE" [22]). Finally, we expanded D to a 2 x 384 matrix by placing zeros in the columns of features that were not among the 120 most highly correlated features.

We used a first-order, low-pass filter to smooth the decoded control vector u_t and determine the gain: $v_{t+1}=\alpha v_t+(1-\alpha)Bu_t$, where v_t is the smoothed control vector at time step t, α is a scalar smoothing parameter (set to 0.96 for virtual reality blocks and 0.9 for FES blocks), and B is a diagonal gain matrix that controls the gain of each dimension separately. The smoothing values were set based upon manual tuning and visual inspection of the resultant motion.

For virtual reality blocks, v_t controlled the velocity of each joint of the virtual arm directly, while for FES blocks v_t was the Decoded Δ Pattern (Supplementary Figure 2) and determined the rate of change of each stimulation pattern's activation percentage (Stimulation Pattern % in Figure 1B and Supplementary Figure 2). In other words, during FES blocks, the new muscle stimulation values at each time step were set equal to the old muscle stimulation values plus v_t multiplied by the time elapsed (20 ms time step). For virtual reality blocks, we set the gains such that at maximum speed (when $u_t=1$), each joint would travel 30% of its range in one second. For FES blocks, we tuned the gain for each joint separately (with values allowing 10 - 30% of a stimulation pattern to be traversed in one second). Supplementary Figure 2 illustrates example time series of important variables during all three conditions (AM, VR, FES) of the VR vs. FES comparison sessions.

Chance Success Rates: Chance success rates for each task (dashed red lines shown in Figure 3 and Supplementary Figure 4) were determined by collecting two additional blocks of the same task while replacing the typical decoder output with phase-randomized decoder output from two previous experimental sessions. The success rate for these two blocks were then averaged together to yield a chance success rate for that task. We randomized the phase of the decoder output by computing a discrete Fourier transform of the time series, randomizing the angle of each coefficient (drawing from a uniform distribution), and then computing an inverse Fourier transform to yield a new time series with the same frequency content but a different phase content that was unrelated to the target locations. Example trajectories resulting from this procedure are shown in Supplementary Figure 6.

Electrogoniometer Calibration: Electrogoniometers (Biometrics Ltd.-US, Ladysmith, VA) were placed on the joint(s) of interest and the range of attainable values was found by using an automatic routine that stimulated each joint automatically, driving it through its range of motion. During FES performance evaluation, joint angle targets spanned 70% to 85% of this range (a reduced range was used to minimize the effect of muscle fatigue). To map recorded voltage to joint angle, we passively stepped each joint through its range of motion while measuring the physical angle.

Stimulation Pattern Design: Before designing the stimulation patterns, we first profiled each electrode by stimulating it individually and noting the resultant joint motion. Then, we designed each pattern manually by grouping together electrodes that were profiled to

produce the desired motion. The timing and relative blending of each electrode was determined manually based on our expertise and visual examination of the resultant motion. These stimulation patterns sometimes changed during the course of the study as we optimized them for performance. The manual design of these stimulation patterns is an established method that has been implemented in previous FES hand and arm systems[20]. To improve control, we sometimes used an automatic routine that first recorded the equilibrium position of the joint at different increments of the stimulation pattern, then "warped" the pattern to make joint equilibrium position a linear function of stimulation pattern activation (Supplementary Figure 8).

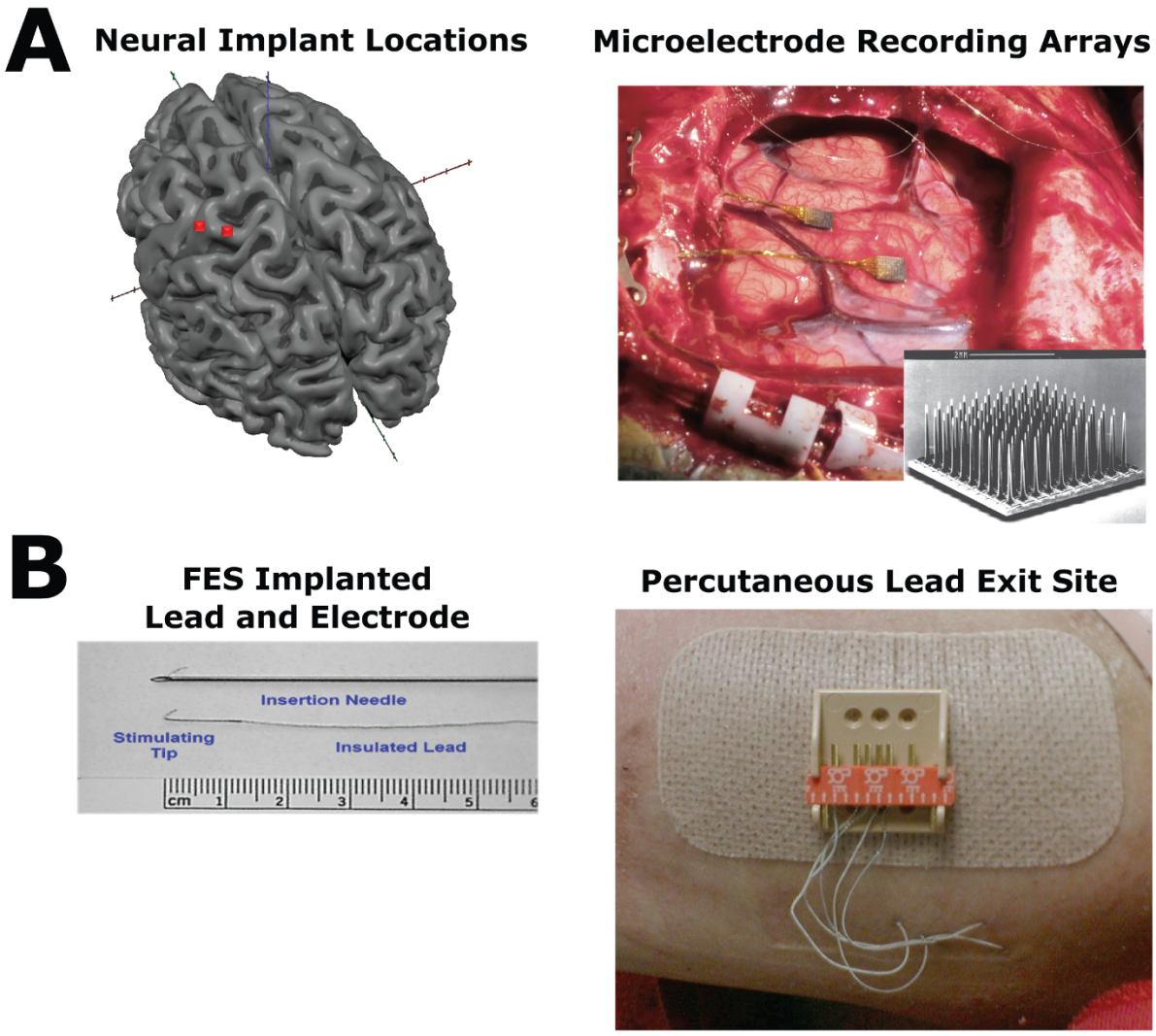

Supplementary Figure 1. Cortical and FES implants. (A) [Left] Structural MRI scan of the participant's brain. The implant locations of the two intracortical arrays are indicated with red squares. Both arrays were surgically targeted to the "hand" area of motor cortex. [Top Right] Photo of microelectrode arrays and wire bundles shortly after intracortical implantation. [Bottom Right] SEM of an example microelectrode recording array (Photo courtesy of Blackrock Microsystems). (B) Example FES implanted lead and electrode [Left]. The insulated leads exited the skin, where pins were attached and placed into connectors [Right] that allowed external cables to interface with the external stimulator. The stimulating tips were surgically targeted to specific muscles (Supplementary Table 3) to achieve the desired elbow, wrist and hand movements.

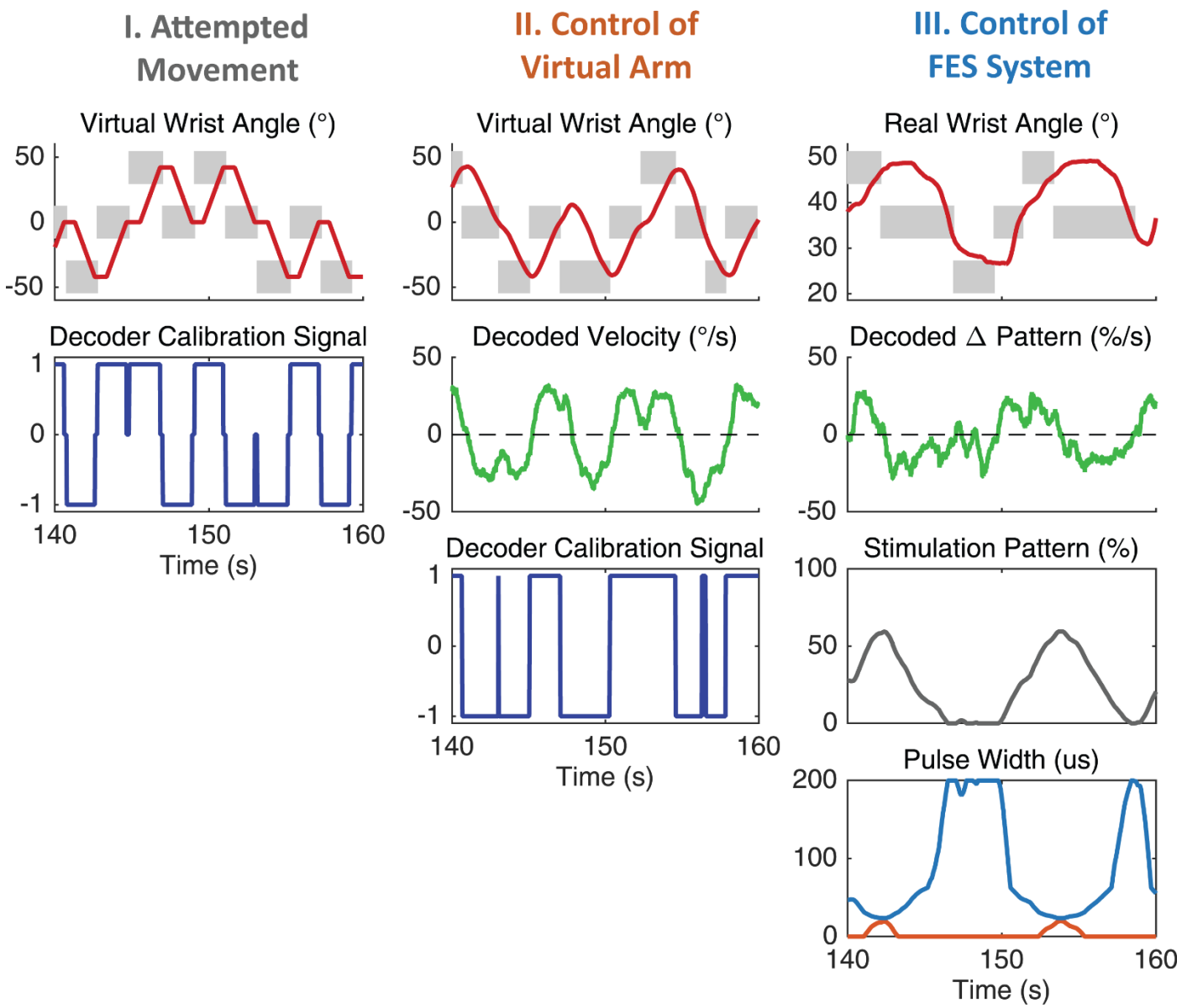

Supplementary Figure 2. Example time series from blocks of single-joint wrist flexion/extension movements made during a VR vs. FES comparison session. Gray squares indicate target joint angles. In condition I, the participant attempts to make the wrist movements shown on screen (illustrated in red). Afterwards, a decoder is calibrated to predict the "decoder calibration signal" (illustrated in blue) from the neural activity. The calibration signal represents the desired direction of joint motion and serves to define what the output of the decoder "should" be. In condition II, the participant uses that decoder to make virtual wrist movements by controlling the angular velocity of the wrist joint (illustrated in green) to acquire wrist position targets. In condition III, we enable the participant to make FES movements of his own wrist by mapping the output of the decoder to the change in stimulation pattern activation (illustrated in green). The pattern activation level itself ("Stimulation Pattern %, illustrated in gray) is the result of integrating the "Decoded Δ Pattern" signal, and can range from 0% (full extension stimulation) to 100% (full flexion stimulation) and determines the pulse widths applied to each FES electrode (illustrated in blue and orange).

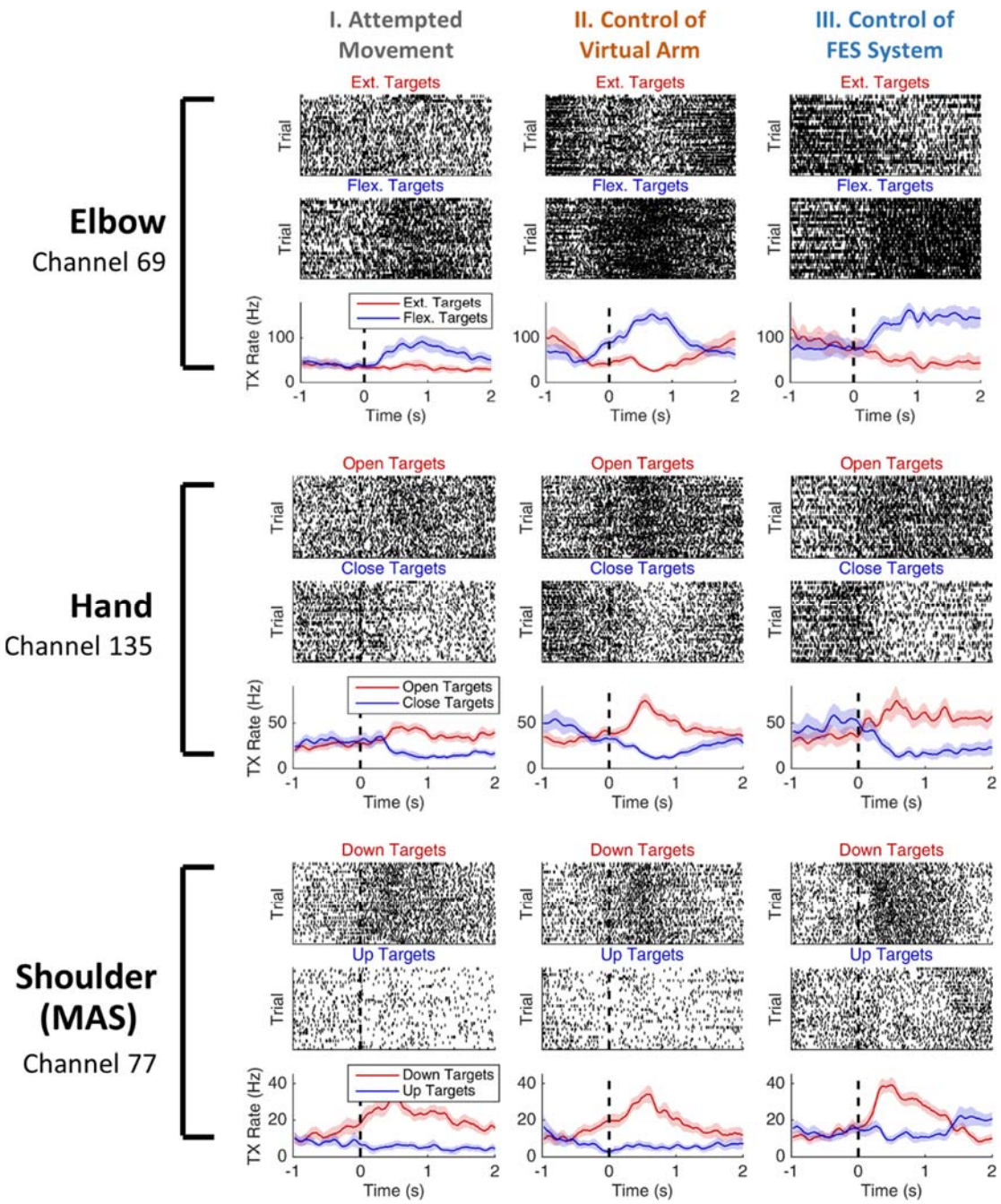

Supplementary Figure 3. Examples of channels that were tuned to single-joint elbow, hand, and shoulder movements during all three experimental conditions. Consistency of tuning across several channels for the three conditions allowed for development of decoders during virtual arm training that were used to initialize decoders during FES arm movements for the VR vs. FES comparison sessions.

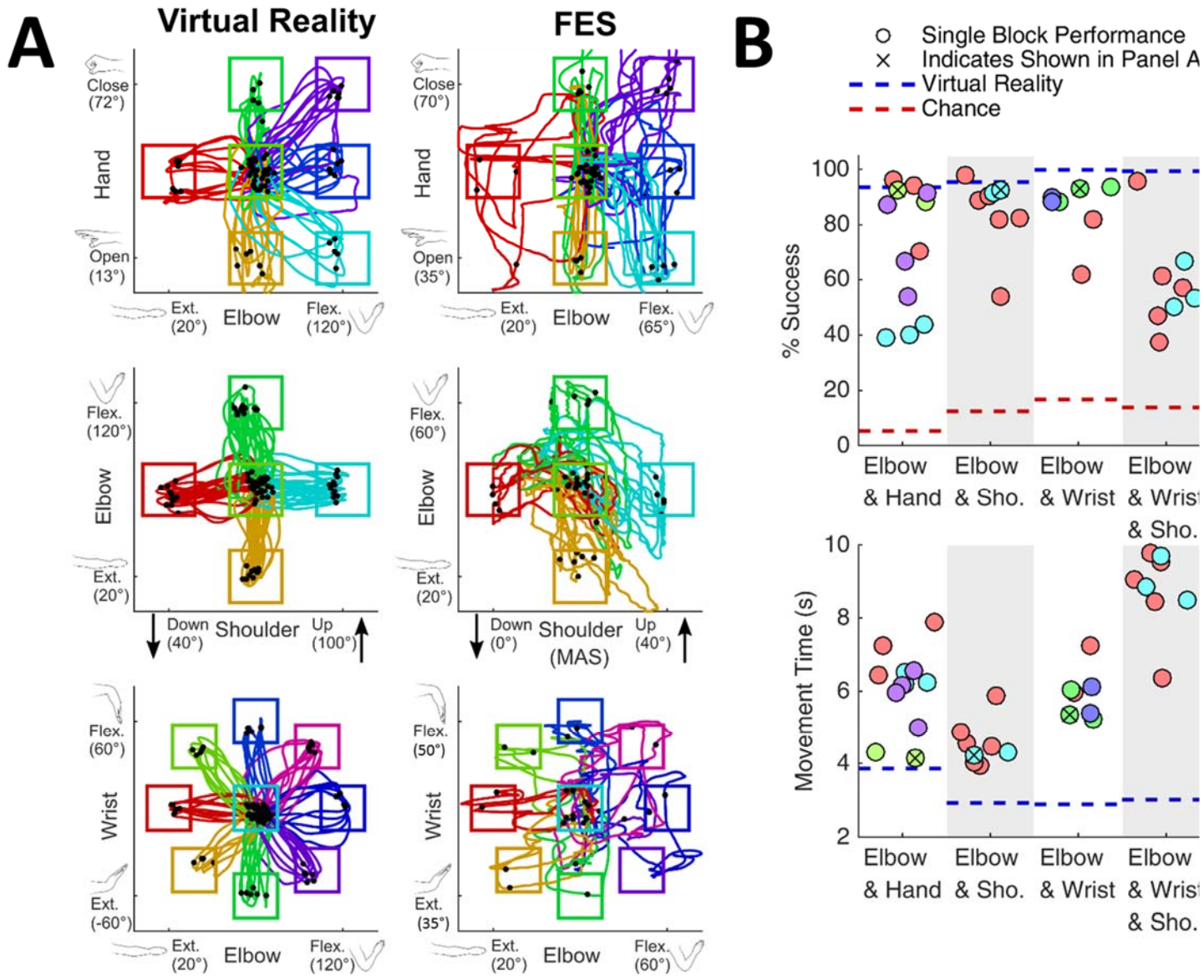

Supplementary Figure 4. Multi-joint FES and mobile arm support (MAS) movements under real-time brain control. (A) Example virtual reality (left column) and FES (right column) movements for each of the two-joint tasks (rows). Each target is drawn as a colored rectangle whose size indicates the tolerance allowed for successful acquisition. Each line corresponds to a single movement and is colored to match its target. Targets and trajectories are plotted in joint space, where each axis is a joint angle (trajectories were generated by plotting the joint angles recorded at each time step on the 2D plane and connecting them with a line). Black dots represent the termination points of the reach trajectories in joint angle space. Blocks with high success rates were chosen for illustration. For the elbow and hand task, we did not test hand open/close movements when the elbow was extended because hand movements were difficult to see at full arm extension in the VR environment. For the elbow and shoulder task, we omitted off-axis targets due to the participant's inability to fully flex his elbow when the arm was fully raised, due to an interaction with the mobile arm support. (B) Success rate and average movement time is summarized for each FES block (circles). Circles are different colors if they occurred on different days. Average virtual reality performance (blue dotted line) and chance performance (red dotted line) are shown for reference.

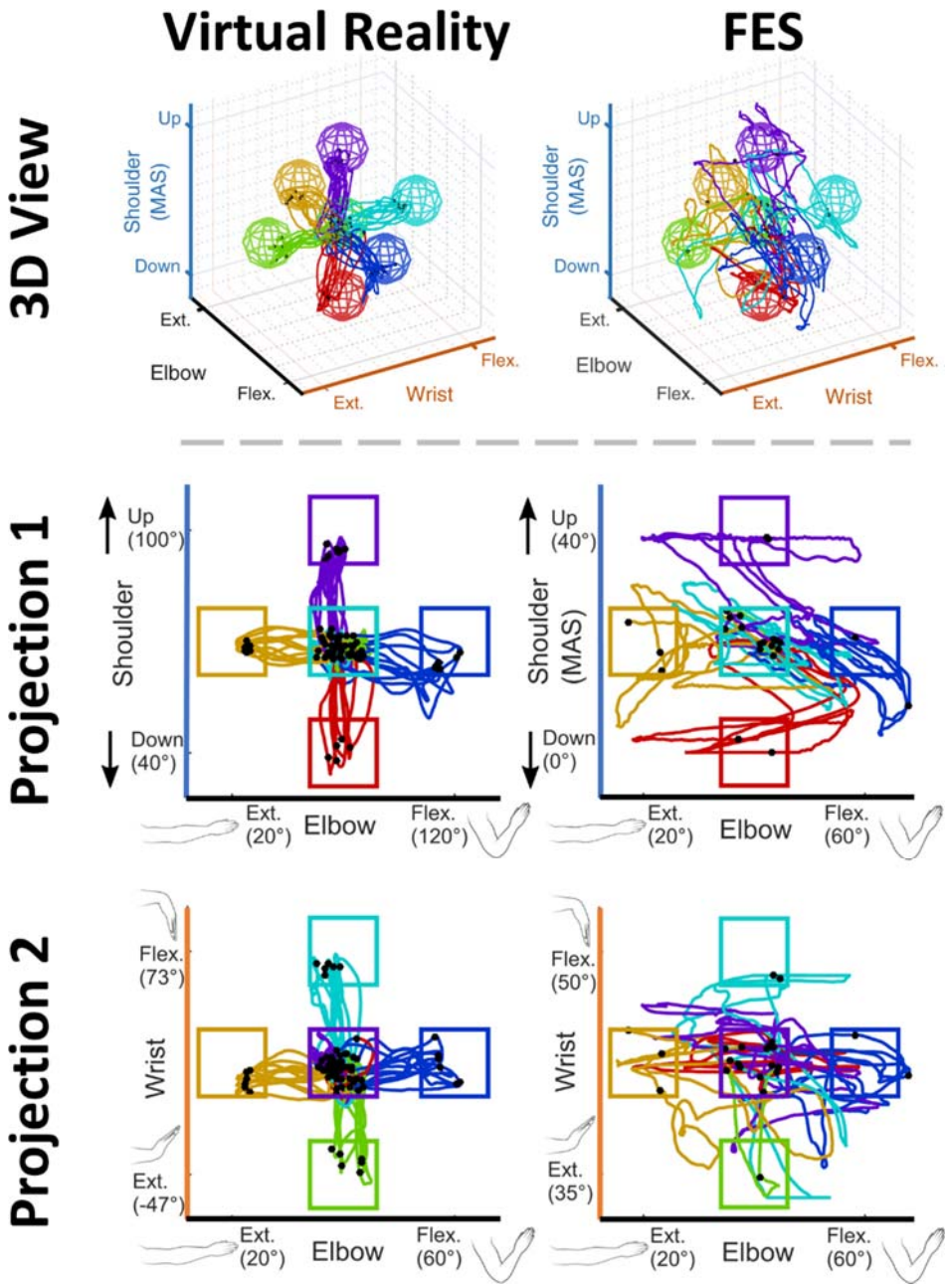

Supplementary Figure 5. Example movement trajectories made during the simultaneous control of three joints (elbow, wrist, and MAS) from a virtual reality block (left column) and an FES block (right column). Black dots represent the termination points of the reach trajectories in joint angle space. The top row plots the trajectories in 3D space while the bottom rows show different two-dimensional projections. The FES block illustrated in the right column is the block with the highest success rate shown in Figure 3B. Note that we only tested 6 targets because including off-axis targets would have added 8 (2^3) more targets, making for too few repetitions per target given the number of movements we were able to collect per session.

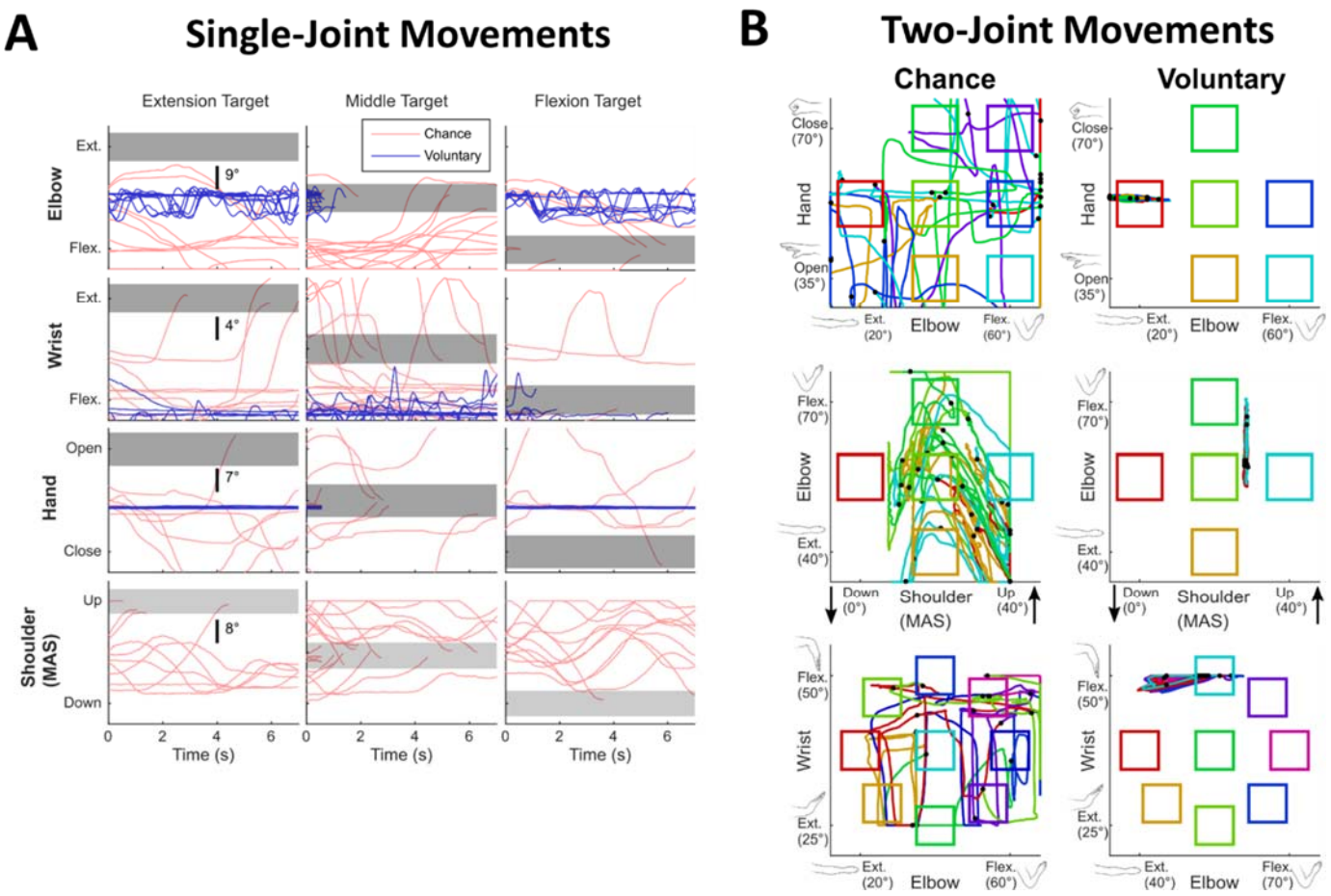

Supplementary Figure 6. Example single-joint (A) and two-joint (B) movements from the chance and voluntary movement blocks. Chance movements were generated by replaying phase-randomized decoded command signals from previous blocks as input to the FES system. The resulting motions have a similar frequency content to brain-controlled FES movements but no relationship to the target, yielding an estimate of what kinds of motions and target acquisitions could be expected "by chance" if brain signals were random and unrelated to the target. Voluntary movements were made by the participant with the FES system turned off and represent the extremely limited arm motions he can make by using his residual shoulder movement.

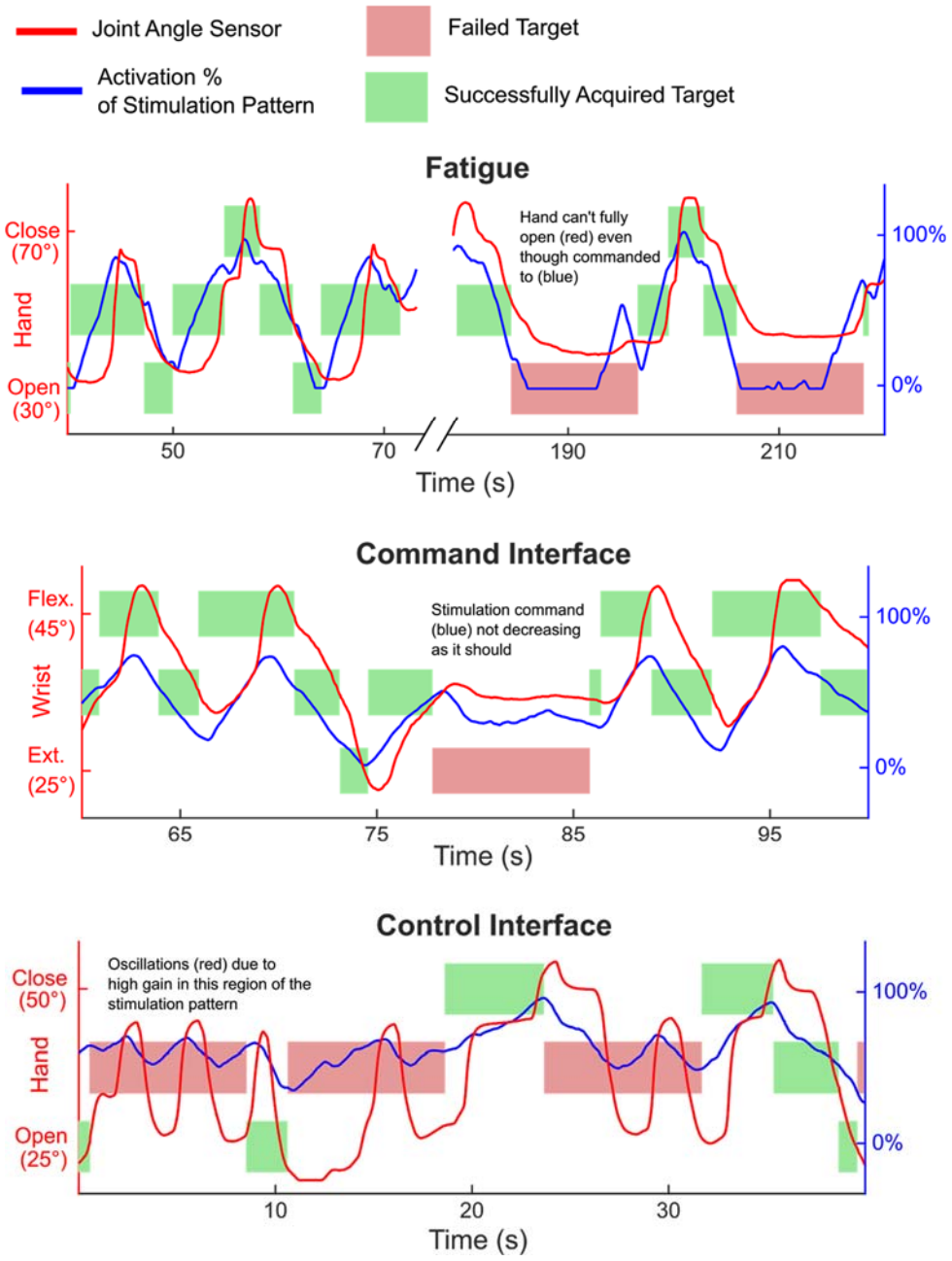

Supplementary Figure 7. Example time series of single-joint movements illustrating the three failure modes (see Supplementary Table 2 for the number of trials categorized in each failure mode): (A) fatigue, (B) poorly decoded command signals, and (C) limitations of our pattern-based control interface. Joint angles (red lines) and corresponding stimulation pattern activation levels (blue lines) are plotted on top of the target regions (green and red rectangles). Acquired targets are green and failed targets are red.

(A) We coded a trial for fatigue if the activation level of the stimulation pattern was at 0 or 100% but the joint could not reach the target. In the example, the hand is initially able to open enough to acquire the "open" targets but later becomes too fatigued.

(B) We coded a trial for command interface (or "decoding") failure if the activation level of the stimulation pattern did not consistently change in the right direction (e.g. did not move more towards extension for an extension target). In the example, the activation level hovers near the middle and even moves in the opposite direction. As a result, the wrist does not extend and the trial is failed.

(C) We coded a trial for control interface failure if the command signal moved in the correct direction but the corresponding joint overshot the target instead of slowing down or stopping accurately in the target region. We also coded for control interface if the movement of one joint caused other joints to move in the wrong direction due to coupling dynamics (common with multi-joint movements that included the mobile arm support). Overshooting and coupling between joints are two problems that our control interface does not compensate for. In theory, a well-designed control system could compensate for these properties, enabling the user to make accurate movements without requiring the user to adapt their command signal. In the example given, the command signal

moves in the correct direction but the hand oscillates around the middle target instead of slowing down within the target region to acquire it. In this case, oscillation occurs due to a non-linear relationship between pattern activation level and hand movement: some regions of the pattern contain little or no sensitivity, while one region near the center is too sensitive and causes uncontrolled motion.

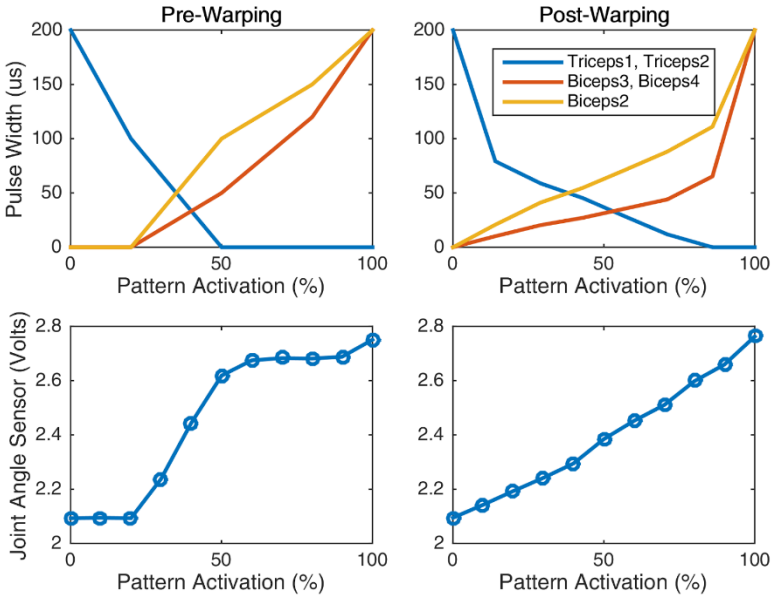

Supplementary Figure 8. Stimulation pattern warping. We employed an automatic procedure to warp a stimulation pattern so that the joint equilibrium position is a linear function of pattern activation. The left column illustrates a manually designed pattern (top row) whose equilibrium positions are a highly non-linear function of pattern activation (bottom row). Our warping procedure enlarges the sensitive region of the pattern (top row) to linearize the equilibrium positions (bottom row).

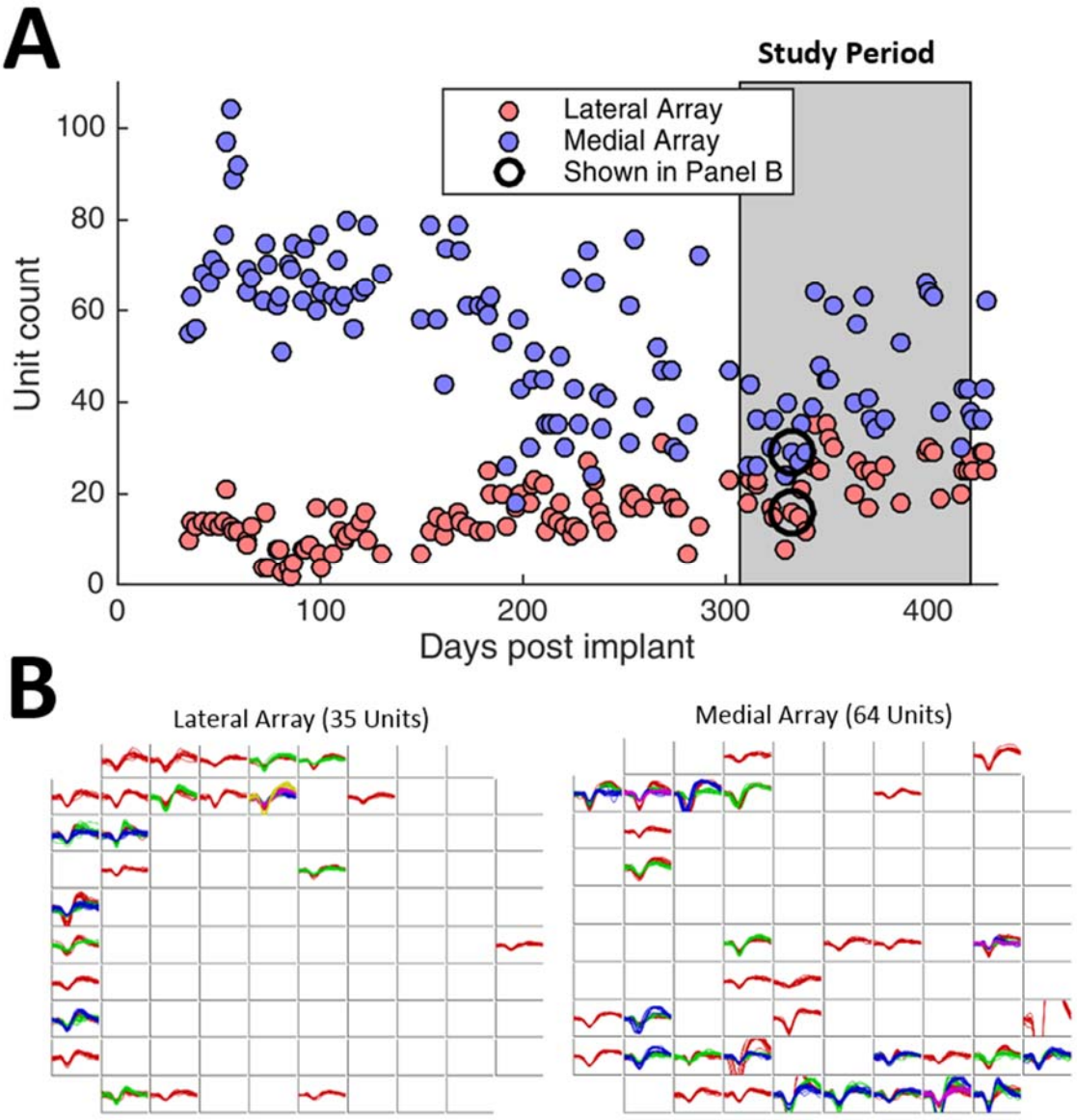

Supplementary Figure 9. Unit counts for each microelectrode array estimated with an automatic offline spike sorting algorithm applied to data during the attempted movement condition (A) and example spike panels showing sorted waveforms from each identified unit on an example day (B).

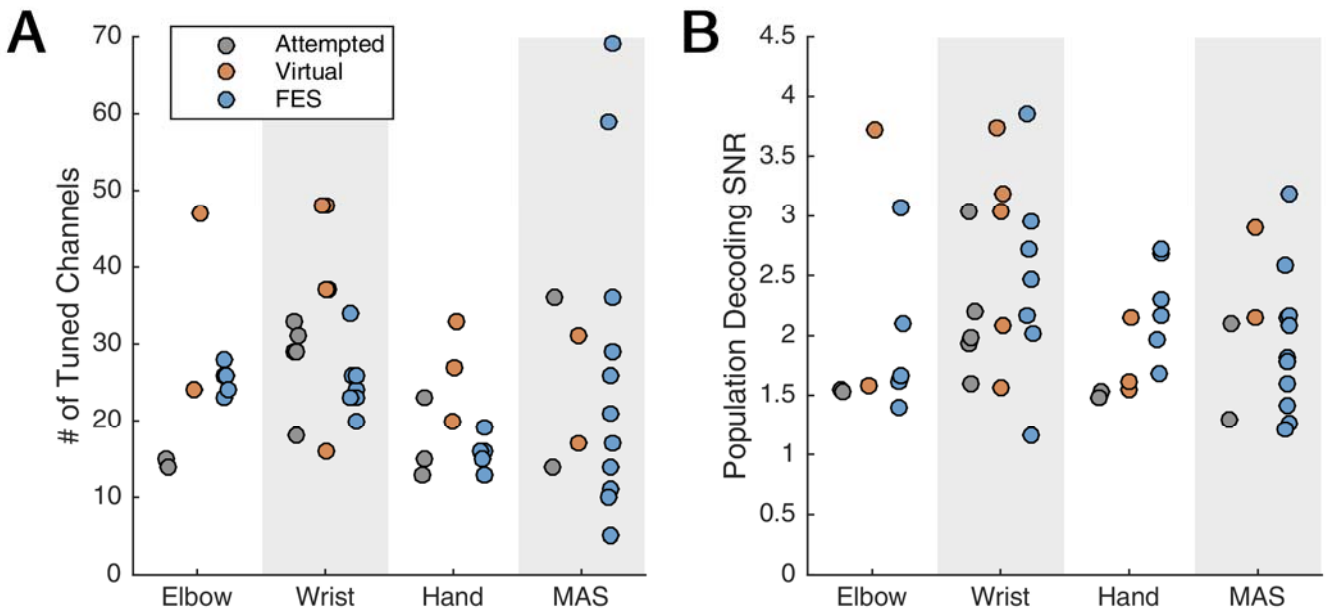

Supplementary Figure 10. A neural tuning analysis performed on all blocks of single-joint movement included in the study. Results show that there was significant tuning to each joint and each condition, though the quality of the tuning varied substantially from block to block.

(A) The number of channels where either the threshold crossing rate or the high frequency spike power was significantly tuned to a given movement (elbow, wrist, hand or MAS) during the given condition (attempted movement, control of the virtual arm, or control of the FES system). Each circle shows the results from a single block. We considered a neural feature to be "tuned" to a certain movement if that feature's mean value was significantly different (t-test, $p<10^{-3}$) between the two opposing commands, such as hand opening versus closing. For each trial, we averaged the feature within a 300 ms window occurring at the beginning of the movement (but after the participant's reaction time of 340 ms), yielding a single data point for each trial. The t-test was performed on these individual trial averages.

(B) The signal-to-noise ratio of a cross-validated (10-fold) linear decoder, which gives a measure of how well we were able to extract information about joint movement from the entire neural population. The decoder was calibrated on each block using the methods described in Supplemental Methods and was applied to the data offline. To measure the SNR, we averaged the *unsmoothed* decoder output (u_t) during a 300 ms window occurring at the beginning of the movement (but after the participant's reaction time of 340 ms), yielding an average decoder output for each trial. We modeled the average output as the sum of decoding error plus a one-dimensional vector pointing from the current joint angle to the target joint angle. We fit the following linear model:

$$u_i = b_0 \frac{g_i - p_i}{|g_i - p_i|} + \varepsilon_i$$

where u_i is the averaged decoder output for trial i, g_i is the target joint angle, p_i is the current joint angle, b_0 is a model parameter and ε_i is Gaussian noise. We fit b_0 and the standard deviation of the noise (σ) using least squares regression and computed the SNR as b_0/σ.

Date	Day Post Implant	Elbow	Wrist	Hand	MAS	Elbow & Hand	Elbow & MAS	Elbow & Wrist	Elbow & Wrist & MAS
2015.10.08	311		1						
2015.10.09	312			2					
2015.10.12	315			1					
2015.10.13	316	1				3			
2015.10.19	322	2							
2015.10.20	323	1			1				
2015.10.26	329			1					
2015.10.30	333			2					
2015.11.02	336		2						
2015.11.03	337					2			
2015.11.05	339					3			
2015.11.09	343						6		
2015.11.10	344					4	2		
2015.11.12	346							2	
2015.11.16	350							3	5
2015.11.17	351							2	3
2015.11.23	357	Chance and Voluntary Motion (2 chance and 1 voluntary block per game)							
2015.11.24	358								
2016.01.25	420	1	1	1	1				
2016.01.26	421		1						
2016.03.08	463	Quantified Functional Coffee Drinking Task							
TOTAL	20	5	5	7	2	12	8	7	8

Date	Day Post Implant	Video Collection Tasks
2015.11.03	337	Video 2: Multi-Joint Movements
2015.12.28	392	Video 4: Functional Coffee Drinking Task
2016.01.07	402	Video 3: 3D Audio Cued Movements
2016.01.25	420	Video 1: Single-Joint Movements
2016.01.26	421	Videos 1 & 3: Single-Joint Movements and 3D Audio Cued Movements
2016.11.07	717	Video 5: Functional Self-Feeding Task

Supplementary Table 1. (Top) Session table indicating the number of blocks of each task completed on each day. Each block was approximately 4 minutes in length, resulting in 39 ± 20 movement attempts per block. (Bottom) Session table indicating the number of days post implant each supplemental video was collected.

Game	Fatigue	Command Interface Only	Control Interface Only	Command & Control Interface
Elbow	0 (0%)	0 (0%)	3 (100%)	0 (0%)
Wrist	1 (33%)	2 (67%)	0 (0%)	0 (0%)
Hand	3 (13%)	0 (0%)	21 (88%)	0 (0%)
Shoulder (MAS)	0 (0%)	0 (0%)	3 (100%)	0 (0%)
Elbow & Hand	0 (0%)	27 (32%)	48 (56%)	10 (12%)
Elbow & Sho.	4 (9%)	4 (9%)	28 (65%)	7 (16%)
Elbow & Wrist	16 (59%)	5 (19%)	7 (26%)	0 (0%)
Elbow & Wrist & Sho.	5 (9%)	16 (30%)	22 (42%)	11 (21%)
Total	**29 (12%)**	**54 (22%)**	**132 (55%)**	**28 (12%)**

Supplementary Table 2. Breakdown of the causes for failed trials during each game. Supplementary Figure 7 gives an example of each failure mode and its definition.

Muscle	# of Electrodes
Anterior Deltoid	2
Middle Deltoid	1
Posterior Deltoid	4
Pectoralis Major	2
Triceps	2
Biceps	3
Extensor Carpi Radialis Longus	2
Extensor Carpi Ulnaris / Extensor Digitorum Communis	1
Flexor Carpi Radialis	1
Flexor Carpi Ulnaris	1
Extensor Digitorum Communis	2
Extensor Indicis Proprius / Extensor Digitorum Communis	1
Flexor Digitorum Superficialis	1
Abductor Pollicis Brevis	1
Abductor Pollicis Brevis / Flexor Pollicis Brevis	1
Adductor Pollicis	2
Extensor Pollicis Longus	4
Flexor Pollicis Longus	1

Supplementary Table 3. A list of all implanted muscles and the number of FES electrodes that stimulate it. For each electrode, the main muscle it activates was estimated by the surgical target and visual examination of the effect of stimulation. Four anodes were also implanted, one near each connector (forearm proximal, forearm distal, upper arm, shoulder), for a total of 36 implanted electrodes.

Success Rates

Condition	Elbow	Wrist	Hand	MAS	Elbow & Hand	Elbow & MAS	Elbow & Wrist	Elbow & Wrist & MAS
FES	0.95	0.97	0.89	0.99	0.66	0.75	0.86	0.61
VR	0.99 *	0.99	1 *	1	0.95 *	0.97 *	0.99 *	0.99 *
Chance	0.45 *	0.33 *	0.63 *	0.62 *	0.075 *	0.13 *	0.17 *	0.15 *

Movement Times

Condition	Elbow	Wrist	Hand	MAS	Elbow & Hand	Elbow & MAS	Elbow & Wrist	Elbow & Wrist & MAS
FES	3.4 ± 2.3	3.4 ± 1.6	4.1 ± 2.9	2.7 ± 1.5	6.6 ± 3.4	6.4 ± 4.1	5.8 ± 3	8.6 ± 3.8
VR	2.1 ± 0.87 *	2.6 ± 1.1 *	2.3 ± 1 *	2.5 ± 1.1	3.7 ± 1.6 *	2.8 ± 1.3 *	2.9 ± 0.94 *	3 ± 0.9 *
Chance	5.5 ± 3.2 *	6 ± 3 *	5.5 ± 3.7 *	4.7 ± 3 *	9 ± 2.1 *	7.5 ± 1.5	11 ± 2.9 *	11 ± 2.4 *

Supplementary Table 4. Mean success rates (top table) and movement times (bottom table) for all FES, VR, and Chance movements pooled together across blocks within each combination of joints tested. In the movement time table, mean ± SD is reported. For each joint combination, we compared the FES success rates and movement times to the VR and Chance success rates and movement times using a two sample binomial test and a t-test. P-values ≤ 0.001 are indicated with an asterisk. Higher success rates and lower movement times in VR vs FES may be attributable to more practice in VR (65 vs. 15 hours), but may have also been caused by the more difficult control task presented by an FES-activated arm: dynamics due to arm mass, muscle contractile properties, interactions between joints, and MAS motor dynamics.

Supplementary Video 1

FES+iBCI single-joint movements done with virtual reality feedback (for comparison with virtual reality arm movements). Video taken 420 and 421 days post implant.

Supplementary Video 2

FES+iBCI multi-joint movements (elbow and hand) done with virtual reality feedback (for comparison with virtual reality arm movements). Decoder output, stimulation patterns, and joint angle measurements are illustrated. Video taken 337 days post implant.

Supplementary Video 3

FES+iBCI audio-cued single-joint movements done just before the functional task was attempted. Comparison of achievable single-joint movements with FES+iBCI system turned off vs turned on. Video taken 402 and 421 days post implant.

Supplementary Video 4

Functional task video – drinking from a straw. The participant successfully completes a reach-to-grasp movement to acquire a cup of coffee. He brings the cup to his mouth and takes a drink, and then returns the cup. Video taken 392 days post implant; the participant had practiced this task for 6 sessions prior.

Supplementary Video 5

Demonstration of study participant performing a self-feeding task for the first time. Using a modified fork (a standard rehabilitation device), the participant successfully moves his arm and hand between a plate of mashed potatoes and his mouth, taking several bites.